ACSNANO
www.acsnano.org
ARTICLE

Graphene Electronic Tattoo Sensors

Shideh Kabiri Ameri,[†] Rebecca Ho,[§] Hongwoo Jang,[⊥] Li Tao,[†,‡] Youhua Wang,[∥] Liu Wang,[∥] David M. Schnyer,[#] Deji Akinwande,[*,†,⊥] and Nanshu Lu[*,†,§,⊥,∥]

[†]Deparment of Electrical and Computer Engineering, [§]Department of Biomedical Engineering, [⊥]Texas Materials Institute, [∥]Department of Aerospace Engineering and Engineering Mechanics, and [#]Department of Psychology, University of Texas at Austin, Austin, Texas 78712, United States

[‡]School of Materials Science and Engineering, Southeast University, Nanjing 211189, China

S *Supporting Information*

ABSTRACT: **Tattoo-like epidermal sensors are an emerging class of truly wearable electronics, owing to their thinness and softness. While most of them are based on thin metal films, a silicon membrane, or nanoparticle-based printable inks, we report sub-micrometer thick, multimodal electronic tattoo sensors that are made of graphene. The graphene electronic tattoo (GET) is designed as filamentary serpentines and fabricated by a cost- and time-effective "wet transfer, dry patterning" method. It has a total thickness of 463 ± 30 nm, an optical transparency of ~85%, and a stretchability of more than 40%. The GET can be directly laminated on human skin just like a temporary tattoo and can fully conform to the microscopic morphology of the surface of skin *via* just van der Waals forces. The open-mesh structure of the GET makes it breathable and its stiffness negligible. A bare GET is able to stay attached to skin for several hours without fracture or delamination. With liquid bandage coverage, a GET may stay functional on the skin for up to several days. As a dry electrode, GET−skin interface impedance is on par with medically used silver/silver-chloride (Ag/AgCl) gel electrodes, while offering superior comfort, mobility, and reliability. GET has been successfully applied to measure electrocardiogram (ECG), electromyogram (EMG), electroencephalogram (EEG), skin temperature, and skin hydration.**

KEYWORDS: *graphene, electronic tattoo, epidermal electronics, wearable electronics, biosensor*

Long-term wearable biometric sensors with high fidelity have the potential to be applicable outside of hospital and lab settings to allow for very broad modes of use, including mobile health care, fitness tracking, human−machine interactions, and so on.[1−3] However, existing medical sensors are too restraining, and the technology is expensive to process the multitude of physiological signals. For example, traditional technologies for electrophysiological measurements use thick, flat electrodes, which are taped to the surface of the skin and have terminal connections to stationary data acquisition facilities.[4] The skin is prepared by light abrasion, and conductive gel or paste is applied at the electrode−skin interface to reduce the contact impedance.[5] Such procedures are time-consuming and unsuitable for long-term (*e.g.*, multiday) recording, since signal quality decays as the gel dries out with time and the gel can be irritating to the skin.

The emergence of wearable electronics provides the opportunity for continuous and ambulatory monitoring. However, their functionality and signal quality are still limited. In fact, commercially available wearable devices are still in the form of rigid electrode sensors and chips mounted on bands or straps to be worn on the wrist, chest, *etc.* They are capable of activity tracking, heart rate recording, and even bioimpedance measurements, but the data quality is still far from medical grade.

Epidermal electronics or electronic tattoos (E-tattoos) are recently developed wearable electronics that are hair-thin and skin-soft, allowing them to intimately couple with human skin for long-term, high-fidelity biometric sensing. Possible applications include but are not limited to continuous recording of electrophysiological signals, skin temperature, skin hydration, oxygen saturation level, and biomarkers in sweat.[6−12] In addition to being lightweight and soft, intimate sensor−skin integration is a major advantage of E-tattoos. As skin is microscopically rough, theoretical analysis has clearly predicted that only ultrathin and ultrasoft tattoos can fully conform to natural skin morphology without artificial adhesives.[13,14] Such conformability enlarges the contact area between the dry electrode and skin and hence lowers the contact impedance, which directly leads to a higher signal-to-noise ratio (SNR) in recorded electrophysiological signals and less susceptibility to motion.[3,15] Gold, a biocompatible and nonirritating material, has been the most popular choice for dry electrodes and interconnects in E-tattoos. Its thickness is often in the range of tens to hundreds of nanometers, and it is supported by translucent polyimide of greater thickness for mechanical robustness.[15] However, gold is too pricy to be used in disposable E-tattoos. Moreover, such sensors are obviously

Received: March 29, 2017
Accepted: July 18, 2017
Published: July 18, 2017

DOI: 10.1021/acsnano.7b02182
ACS Nano XXXX, XXX, XXX−XXX

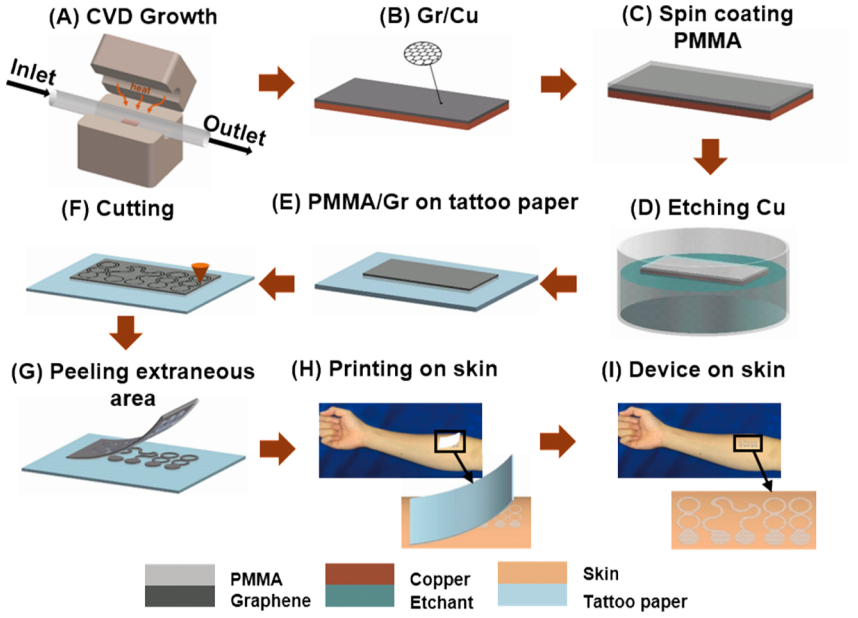

Figure 1. Fabrication process of GET. (A, B) Graphene was grown on copper foil using atmospheric pressure chemical vapor deposition system (APCVD). (C) Less than 500 nm thick PMMA was spin coated on graphene. (D) Copper was etched away. (E) Graphene/PMMA (Gr/PMMA) was transferred onto tattoo paper with PMMA touching the paper and graphene facing up. (F) Gr/PMMA was cut by a mechanical cutter plotter. (G) Extraneous Gr/PMMA was peeled off from the tattoo paper. (H) Mounting GET on skin like a temporary transfer tattoo. (I) GET on skin.

visible, which makes it unsuitable to wear on parts of the body such as the face.

As the thinnest electrically conductive material, graphene is optically transparent, mechanically robust, electrochemically stable, and biocompatible.[16−22] It has therefore been successfully used in a tooth-integrated wireless bacteria detector, a flexible and transparent electrode array for simultaneous electrocorticography (ECoG) recordings and neuroimaging measurement of skin impedance and temperature and movement detection .[23−27] However, the total thicknesses of these graphene-based sensors are tens or hundreds of micrometers, which is too large to fully conform to the skin like a real tattoo. Moreover, while the aforementioned graphene biosensors were successfully patterned by photolithography, the process can be costly and time-consuming. The recently developed freeform "cut-and-paste" process can be modified and employed to pattern chemical vapor deposited (CVD) large area graphene.[28]

In this work, we have developed a stretchable and transparent graphene based electronic tattoo (GET) sensor that is only sub-micrometer thick but demonstrates high electrical and mechanical performance. We demonstrate that a GET can be fabricated through a simple "wet transfer, dry patterning" process directly on tattoo paper, allowing it to be transferred on human skin exactly like a temporary tattoo, except this sensor is transparent. Due to its ultrathinness, a GET can fully conform to the microscopic morphology of human skin *via* just van der Waals interactions and can follow arbitrary skin deformation without mechanical failure or delamination for an extended period of time. Because of the open-mesh design of the filamentary serpentines, the GET is breathable and has negligible mechanical stiffness. It is, therefore, almost imperceptible both mechanically and optically. GET has been used for various physiological measurements including electrocardiogram (ECG), electromyogram (EMG), electroencephalogram (EEG), skin temperature, and skin hydration, each of which has been validated by a corresponding gold standard sensors.

RESULTS AND DISCUSSION

The "wet transfer, dry patterning" fabrication process is illustrated in Figure 1. "Wet transfer" refers to the copper etching step, which retains the high continuity of the large-area graphene grown on copper foil. "Dry patterning" refers to the use of a programmable mechanical cutter plotter to carve out the designed filamentary serpentine shapes on the graphene. Compared with photolithography, the dry patterning process minimizes the chemical contamination of graphene and is significantly more time- and cost-effective. Stepwise, graphene was first grown on a copper foil using atmospheric pressure chemical vapor deposition (APCVD) as previously reported (Figure 1A).[29] As-grown CVD graphene on copper foil (Figure 1B) was characterized by scanning electron microscopy (SEM) and Raman spectroscopy (Supporting Information Figure S1). The SEM image (Supporting Information Figure S1A) clearly shows adlayers scattered randomly over the monolayer graphene. The Raman spectra at three random spots (Supporting Information Figure S1B) demonstrate the variation of the 2D to G peak ratios due to the difference in the number of graphene layers. The Raman mapping (Supporting Information Figure S1C) and corresponding histogram (Supporting Information Figure S1D) over an area of 100 μm × 100 μm suggest that graphene coverage on copper is about 99%, out of which 30% to 40% has adlayers and the rest is monolayer. We found that the existence of adlayers is beneficial to the continuity of large-area CVD graphene.

To retrieve the graphene from copper, sub-micrometer-thick poly(methyl methacrylate) (PMMA) was spin coated onto the as-grown graphene (Figure 1C), followed by copper etching (Figure 1D) and rinsing with deionized (DI) water. The graphene/PMMA (Gr/PMMA) bilayer was then transferred onto a piece of tattoo paper (Silhouette) with graphene facing

DOI: 10.1021/acsnano.7b02182
ACS Nano XXXX, XXX, XXX−XXX

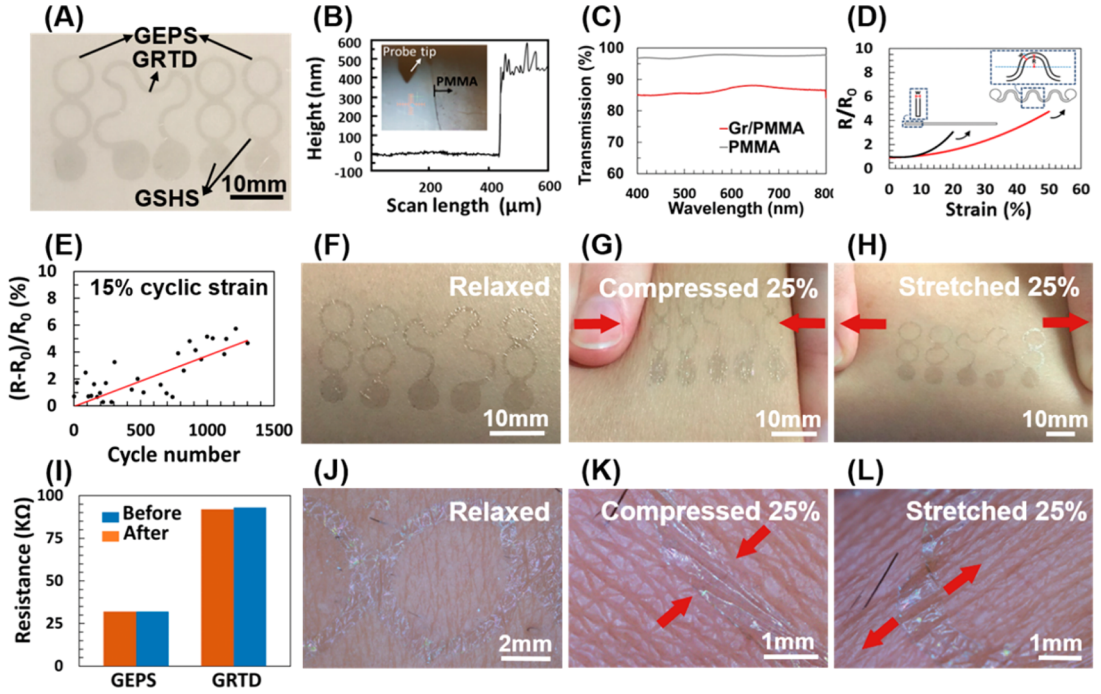

Figure 2. Mechanical and optical characterization of the GET. (A) Picture of the as-fabricated GET with a white background, labeled with different sensors including graphene-based electrophysiological sensors (GEPS), a resistance temperature detector (GRTD), and a skin hydration sensor (GSHS). (B) The thickness of PMMA was measured by a profilometer to be 463 ± 30 nm. (C) Optical transparency of bare PMMA and Gr/PMMA. (D) Normalized resistance of the GET *versus* applied tensile strain. The linear GET ribbon ruptures at 20%, whereas the serpentine-shaped GET can be stretched up to 50%. (E) Less than 6% change in GRTD resistance after 1300 cycles of 15% stretching. (F) GET mounted on skin. (G, H) GET on skin compressed and stretched by 25%, respectively. (I) Change in GEPS and GRTD resistance after all kinds of skin-tolerable deformations. (J to L) Magnified photographs of a GET on relaxed, compressed, and stretched skin, which demonstrate its full conformability even under skin deformation.

up and PMMA in contact with the paper (Figure 1E). The sheet resistance of the Gr/PMMA was measured to be 1994.33 ± 264 Ω/□. Supported by the tattoo paper, the Gr/PMMA bilayer was carved into filamentary serpentine ribbons by a benchtop programmable mechanical cutter plotter (Silhouette Cameo) (Figure 1F). The serpentine ribbons were designed with a width of 0.9 mm and a radius of 2.7 mm to ensure the GET has a stretchability greater than that of skin.[30,31] The extraneous areas of the Gr/PMMA were manually peeled off (Figure 1G), leaving a completed GET sensor on tattoo paper. The fabricated GET sensor can then be transferred onto any part of the glabrous or less-hairy skin, regardless of its curvature or shape, simply by bringing the graphene side in contact with the skin and wetting the backside of the tattoo paper to detach the GET from the paper (Figure 1H), exactly like a temporary transfer tattoo. No skin preparation or skin adhesive is required; the ultrathin GET can stay attached to the skin *via* just van der Waals interactions, as shown in Figure 1I (see Supporting Video VS1 for the process of laminating a GET on the skin).

In addition to transparent PMMA, a popular substrate often used in flexible electronics, polyimide (PI), was also applied to support graphene following a procedure similar to Gr/PMMA. The schematics for the fabrication process of graphene/polyimide (Gr/PI) sensors are shown in Supporting Information Figure S2. As the PI thickness was 13 μm, the Gr/PI sensors cannot stay attached to human skin by just van der Waals interactions. Therefore, the Gr/PI sensors were transferred onto a 3M Tegaderm tape with graphene facing up and then taped onto the skin for measurements. The effect of the sensor's thickness on sensing quality was studied by comparing the functionality of thick nonconformal Gr/PI sensors with that of the ultrathin, conformal GET sensors, which will be discussed later.

A picture of an as-fabricated Gr/PMMA-based GET is shown in Figure 2A, in which different types of physiological sensors are labeled: graphene-based electrophysiological sensor (GEPS), resistance temperature detector (GRTD), and skin hydration sensor (GSHS). The GSHS shares one electrode with the GEPS. The total thickness of the GET was measured to be 463 ± 30 nm using a profilometer (Dektak 6 M Stylus) (Figure 2B). The optical transmittance of Gr/PMMA was measured by a Cary 5000 UV−vis−NIR spectrometer at five random spots over an area of 2 cm × 3 cm (Figure S3A). The average transmittance of PMMA and Gr/PMMA in Figure 2C indicates that within the wavelength range of 400 to 800 nm the transmittance of bare PMMA is 96.5% to 98%, and the transmittance of GET is 84% to 88% due to additional light absorption by graphene.

The mechanical performance of the GET has been analytically modeled and experimentally measured. Neglecting the sub-nanometer-thick graphene layer, the bending stiffness of the GET is essentially that of the supporting PMMA substrate. With a reported Young's modulus of 3.3 GPa, the 463 nm thick PMMA has a bending stiffness of 2.7×10^{-11} N·m, which is an order smaller than the bending stiffness of Au-based ultrathin epidermal electrodes (*e.g.*, 3.49×10^{-10} N·m for 100 nm thick Au on 700 nm thick polyimide).[32] Besides superior flexibility, polymer-supported CVD graphene was reported to have fracture strains around 10%.[33] By performing

DOI: 10.1021/acsnano.7b02182
ACS Nano XXXX, XXX, XXX−XXX

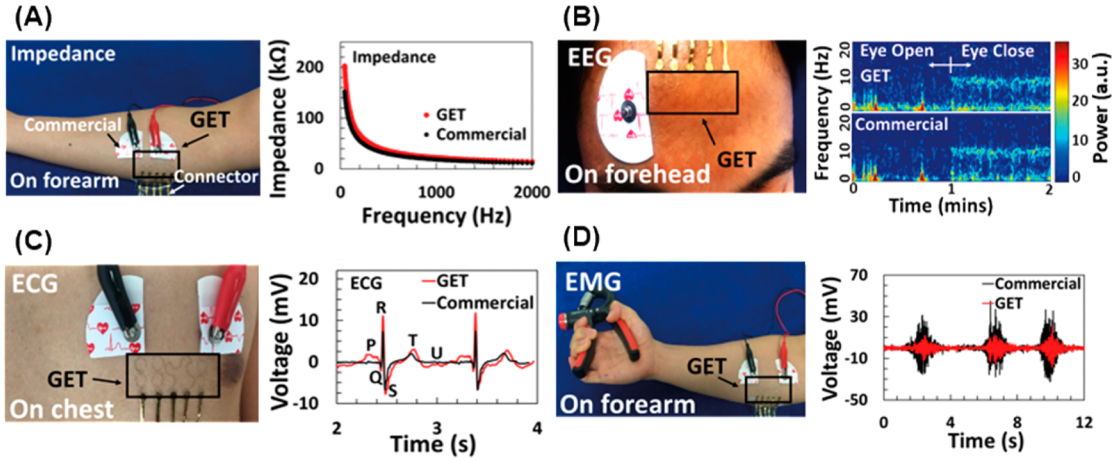

Figure 3. Electrical performance of the GET on skin. (A) Without any skin preparation, GET−skin contact impedance is almost on par with that between commercial gel electrodes and skin. (B) EEG sensing on the forehead with both the GET and gel electrodes (left). When the eyes were closed, an α rhythm of 10 Hz is visible in both spectrograms. (C) ECG measured synchronously by the GET and gel electrodes. Characteristic ECG peaks can be measured by both electrodes. (D) EMG sensing on the forearm with the GET and gel electrodes when the subject squeezed the hand exerciser three times.

uniaxial tensile tests on Gr/PMMA with *in situ* electrical resistance measurement (Figure 2D), we found that the linear Gr/PMMA ribbon ruptures at strains around 20%, while the serpentine-shaped Gr/PMMA ribbon remains electrically conductive up to a strain of 50%, which is well beyond the stretchability of human skin (~30%).[34] The mechanical stiffness of a freestanding GET serpentine ribbon (463 nm thick, 0.9 mm wide, and 2.7 mm in radius) is calculated to be 1.48 N/m according to our previous analytical models, which is less than half of that of the human epidermis (3.9 N/m).[25,26,35] The performance of the GET under a cyclic tensile strain of 15% is demonstrated in Figure 2E, Figure S4, and Supporting Video VS2. The increase in resistance is within 6% after 1300 cycles (Figure 2E).

Figures 2F to H and Supporting Video VS3 offer pictures and a video of the GET on relaxed human skin and skin subjected to various kinds of deformations. Electrical resistance of the GEPS and GRTD was measured before and after arbitrary skin deformation in Figure 2I, and no significant change could be identified. According to an analytical model we built previously, the GET has to be thinner than 510 nm to achieve full conformability with human skin (see Supporting Information Figure S5).[36] With our GET thickness being just 463 nm, optical micrographs of it on skin (Figures 2J−L) confirm the ultraintimate coupling between the GET and skin, even under severe skin deformation.

Electrode−skin conformability directly dictates the contact impedance. Classical electrical circuit concepts suggest that the electrode−skin interface impedance is inversely proportional to the contact surface area.[37] Since conformal contact increases the effective contact area, it is therefore expected that interface impedance decreases. We measured the GET−skin interface impedance and compared it with commercial Ag/AgCl gel−skin interface impedance, the latter of which is considered the gold standard for medical applications. The measurement was performed by laminating a GET on a human forearm without any skin preparation. The GSHS was connected to an LCR meter (Hioki 3532-50) using a customized flexible connector (Supporting Information Figure S6). A pair of Ag/AgCl gel electrodes were placed next to the GSHS with the same interelectrode distance, and the electrodes were connected to the LCR meter by alligator clips, as displayed in Figure 3A. The impedance was measured from 42 Hz to 2 kHz. The result shows that the GET−skin interface impedance is comparable with the gel electrode−skin impedance, although the GSHS surface area (~0.245 cm^2) is more than 10 times smaller than that of the gel electrode (~2.6 cm^2). A similar measurement was conducted with a 13 μm thick Gr/PI electrode of the same shape as GSHS. The Gr/PI electrode had to be held by a 3M Tegaderm tape to stay attached to the skin (Supporting Information Figure S7A). The contact impedance of Gr/PI was more than 1 order of magnitude higher than that of the gel electrode and the GET, which indicates that the 13 μm thick Gr/PI was not able to conform to the skin as well as the 463 nm thick GET.

Low contact impedance is essential for a high SNR in electrophysiological measurements.[38] EEG, ECG, and EMG signals were measured using the GET (Figures 3B−D) and Gr/PI electrodes (Supporting Information Figures S7B−D). The EEG signal was measured by laminating the GET on the forehead next to a commercial gel electrode, as shown in Figure 3B. Reference and ground electrodes were placed on the mastoid bone behind the right ear and on the forearm, respectively. No skin preparation was performed before mounting all the electrodes on the skin. The signal was amplified and recorded using a BrainVision recorder. During EEG measurement, the subject was asked to keep his eyes open for 1 min and then close his eyes for another minute. An alpha rhythm of frequency between 8 and 13 Hz is expected to appear in the EEG when the subject closes his eyes and relaxes. EEG signals recorded in the time domain by both the GET and gel electrodes are displayed in Supporting Information Figure S8A, with a 60 Hz notch filter applied. Spikes in Supporting Information Figure S8A are likely induced by eye blinking because they disappear after eye closure. Fast Fourier transforms (FFT) were performed in MATLAB on EEG signals measured by the GET during eye opening and eye closure. Plots of these results are shown in Supporting Information Figure S8B. The alpha rhythm with a peak at 10 Hz is clearly visible in the eye-closed EEG. It is evident in Figure 3B that the spectrograms of EEGs measured by the GET and gel electrodes are almost identical, and the blinks and alpha

DOI: 10.1021/acsnano.7b02182
ACS Nano XXXX, XXX, XXX−XXX

rhythms are clearly visible in both measurements. Similar experiments were carried out for Gr/PI electrodes (Supporting Information Figures S7B, S8C,D). Comparing the EEG spectrograms measured by Gr/PI and gel electrodes in Supporting Information Figure S7B, it is obvious that the Gr/PI EEG is more noisy, which is also true when we compare the EEG signals in the time domain (Supporting Information Figure S8C).

The GET can also be laminated on the human chest to measure an ECG. Figure 3C shows the measurement setup and the ECG signal recorded by an AvatarEEG through both a GEPS and commercial gel electrodes, with a 60 Hz digital notch filter applied. Characteristic ECG peaks (P, Q, R, S, T, and U) were clearly visible in both sets of data, but the GEPS measurement showed slightly higher signal magnitude. The SNR of the ECG measured by the GEPS was found to be 15.22 dB, which is higher than the SNR of the gel electrodes (11 dB). This can be attributed to the higher surface charge density and surface electric displacement field of graphene compared with Ag/AgCl gel, which results in the more efficient capturing of electrical potential.[39] Similar ECG measurement capabilities have been demonstrated by Gr/PI electrodes, as shown in Supporting Information Figure S7C. However, the data show a considerably higher noise level and the SNR is only 7.2 dB for Gr/PI electrodes.

Application of a GET for EMG measurement was demonstrated by laminating a GET on the human forearm. The electrical activity of the forearm flexor muscle was measured using both the GEPS and commercial gel electrodes when the subject was squeezing a handgrip (Figure 3D). An AvatarEEG was used to record the signal, and a 60 Hz digital notch filter was applied to both sets of recorded EMGs. The difference between the signals measured by the GET and gel electrodes in Figure 3D is attributed to the offset of electrode placement. Gr/PI electrodes have also been applied for EMG measurements, and the comparison with gel electrodes is shown in Supporting Information Figure S7D.

To obtain an in-depth understanding of the effects of conformability on signal strength, circuit models were proposed and simulations were performed for conformal (Supporting Information Figure S9A) and nonconformal (Supporting Information Figure S9B) electrodes using the Microwave Office software. In this simulation, the electrical model of the skin is adopted from a reference. It can be represented by a resistor (R_{sd}), which represents the dermis and subcutaneous layers, in series with a capacitor (C_{se}) and resistor (R_{se}) in parallel, both of which represent the epidermis, as depicted in Supporting Information Figure S9C.[40] In the case of nonconformal electrodes, there are air gaps between the electrode and skin, which can be modeled by another capacitor (C_{gap}) and resistor (R_{gap}) in parallel, as illustrated in Supporting Information Figure S9D. These air gaps increase the contact impedance drastically. When the contact impedance is much lower than the load impedance of the amplifier (*i.e.*, the conformal scenario), the transfer ratio of V_{out} to V_{in} remains close to 1. Otherwise (*i.e.*, the nonconformal scenario), the transfer ratio will drop significantly. Simulation results are presented in Supporting Information Figure S9E.

Another disadvantage of conventional dry electrodes lies in their high susceptibility to motion.[38] However, because of the ultimate skin conformability of the GET, we expect that the dry GET will have motion artifacts comparable with those of gel electrodes. To validate this hypothesis, we placed commercial gel electrodes next to a GEPS on the chest and induced artificial motion in the skin by poking the chest with a glass rod at equal distances from both pairs of electrodes during ECG measurement, as shown in Figures 4A and B. The raw ECG signals recorded using the GET and gel electrodes, displayed in Figure 4C, indeed show similar motion artifacts.

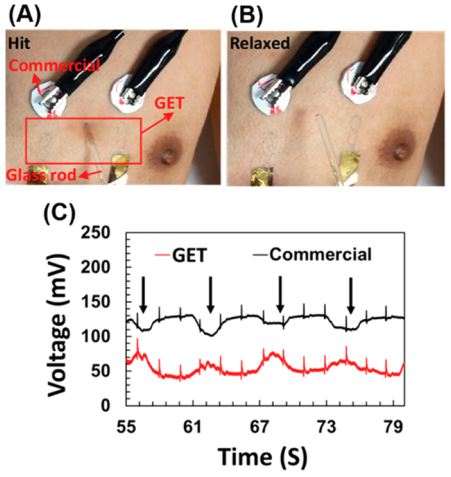

Figure 4. Comparison of motion artifacts in GET and gel electrodes. (A, B) The motion was induced by poking the chest using a glass rod. (C) ECG synchronously recorded by a GET and gel electrodes shows comparable susceptibility to motion.

In addition to electrophysiological measurements, the GET is also able to measure skin temperature and hydration. Previous studies have demostrated that skin hydration level is monotonically correlated with skin impedance.[9] Before performing real-time measurments, we calibrated the GSHS with a commercial corneometer. Skin hydration was tuned by applying body lotion on the skin. As the lotion dried out, the skin hydration level gradually decayed. Every time the skin hydration was measured with the corneometer, the impedance between the two GSHS electrodes was measured using an LCR meter at frequencies between 42 Hz and 1 kHz. The calibration curves are presented in Supporting Information Figures S10A and B. It is evident that the magnitude of impedance increases with decreasing hydration level and that the sensitivity of the GSHS is higher at lower frequencies, as reported by other works.[9,41] To do real-time skin hydration measurement using the GET, body lotion was applied to the skin prior to measurement. Then the skin impedance and hydration level were measured using the GSHS and a corneometer. Using our calibration data, we calculated skin hydration based on the impedance measured by the GSHS and plotted it against the corneometer measurement, as shown in Figure 5A. The GET result parallels the corneometer measurement, which validates the GSHS. Compared with the coneometer, a major advantage of the GET is its wearability and capability of continuous skin hydration measurement. Similar calibration curves (Supporting Information Figures S10C,D) and real-time skin hydration measurements (Supporting Information Figure S7E) were obtained for Gr/PI hydration sensors. The slower decaying rate in hydration measured with Gr/PI (Supporting Information Figure S7E) is attributed to the coverage of the Tegaderm adhesive, which prevents the skin from breathing naturally. In contrast, the open-mesh GET guarantees breathability and hence has a rate

DOI: 10.1021/acsnano.7b02182
ACS Nano XXXX, XXX, XXX−XXX

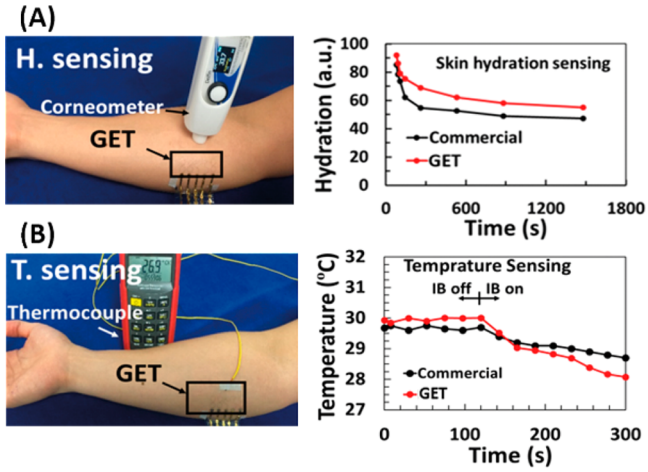

Figure 5. Demonstration of a GET as a skin hydration and skin temperature sensor. (A) Skin hydration sensing right after the application of body lotion, using both a GSHS and a commercial corneometer. GSHS calibration curves are provided in Supporting Information Figure S10. (B) Skin temperature sensing with an ice bag placed in the vicinity of the GRTD and a thermocouple. GRTD calibration curves are provided in Supporting Information Figure S11.

of hydration drop that is comparable with the corneometer measurement (Figure 5A).

Resistance temperature detectors (RTDs) are mostly made of long metal wires whose electrical resistance changes due to the change of temperature, as expressed by the following equation:[28]

$$\frac{\Delta R}{R_0} = \alpha \Delta T \tag{1}$$

where ΔR and ΔT are the change in resistance and temperature, respectively, and α is the temperature coefficient of resistance, which is a material property. For a given temperature change, a large ΔR requires a large R_0. Since metals in general have low electrical resistivity, a large R_0 requires long metal wires or strips. To the contrary, graphene has a sheet resistance that is orders of magnitude higher. As a result, RTDs made of graphene can be much shorter in length and smaller in size. We fabricated a graphene-based filametery serpentine ribbon RTD (GRTD) using this concept, as labeled in Figure 2A, and performed skin temperature measurements. Before real-time measurement, the GRTD was calibrated using a commercial thermocouple by placing it on a hot plate next to the thermocouple and measuring its resistance change as the hot plate temperature ramped up. Eventually the $\Delta R/R_0$ of the GRTD was plotted as a function of ΔT, as shown in Supporting Information Figure S11A. A similar calibration curve for a Gr/PI-based RTD is plotted in Supporting Information Figure S11B. The α coefficient was found to be 0.0042 and 0.0009 $^{\circ}C^{-1}$, respectively. Both coefficients are higher than the graphene-based RTD reported in the literature (0.00015), in which graphene was supported by an epoxy (SU8-2).[42] The discrepancy among the different RTDs indicates that the behavior of graphene is highly dependent on its substrate, which is not surprising considering the large surface-to-volume ratio of graphene. More studies have to be carried out to reveal the underlying mechanisms of different polymer substrates. To validate the GRTD in measuring real-time skin temperature, we laminated the GET on the human forearm and placed a thermocouple next to it (Figure 5B). We then placed an ice bag next to the GET and recorded the change in skin temperature using both the GRTD and the thermocouple (see Supporting Information Figure S7F for the result of the Gr/PI-based RTD). Both results show the skin temperature dropped gradually after placing an ice bag next to it, and close similarities can be found between the GRTD and the thermocouple.

The durability of the GET was tested by laminating it on the forearm and measuring the skin−GET impedance every few hours while the subject maintained normal daily activities (Supporting Information Figure S12). When no tape, adhesive, or liquid bandage was used, the GET stayed conformal to the skin for more than 4 h. The first delamination was observed after 4 h and 23 min (Supporting Information Figures S12F,G). Liquid bandage has been applied by previous researchers to seal electronic tattoos directly printed on the skin.[43] Following this practice, in a second experiment we sprayed less than 1-μm-thick liquid bandage over the GET immediately after it was transferred on the skin (Supporting Information Figures S12H−J). No cracks or delamination was observed for up to 52 h after the transfer, and the contact impedance remained low (Supporting Information Figure S12K). However, 96 h after the transfer a crack was visible in the serpentine ribbon (Supporting Information Figures S12J) and hence the corresponding impedance increased by 1 order of magnitude (Supporting Information Figure S12K). The wearability of the GET during athletic activity was tested by placing three GEPS on different locations including the chest, bicep, and forearm (Supporting Information Figure S13). Liquid bandage was sprayed over one of the electrodes of each GEPS. The subject kept running on a treadmill for 25 min at a speed of 6.5 mph. We did not observe delamination in any of the electrodes after running (Supporting Information Figure S13.) After use, the GET can be easily peeled off from the skin by a piece of adhesive tape (see Supporting Video VS4).

CONCLUSION

We invented a sub-micrometer-thick transparent GET that can function as a stretchable and noninvasive electronic tattoo for multimodal biometric sensing. It is manufactured by a low-cost "wet transfer, dry patterning" process on tattoo paper, which can minimize the chemical contamination of the GET. The GET can be directly transferred on human skin from tattoo paper. Although no adhesive is applied, the GET can fully conform to the microscale morphology of skin and follow arbitrary skin deformation without any fracture or delamination for an extended period of time. The GET was used to measure EEG, ECG, EMG, skin hydration level, and skin temperature. As dry electrodes, the GET−skin interface impedance is almost as low as that of Ag/AgCl gel electrodes, which can be attributed to its ultimate conformability. As a result, the GET has achieved comparable SNR with gel electrodes and also demonstrated similar susceptibility to motion. As tattoo-like wearable skin hydration and temperature sensors, the GET has been validated by state of the art gold standards. We believe that the GET has opened a door for two-dimensional materials to be applied in biosensing electronic tattoos, as well as many other applications.

METHODS

Fabrication of the GET. Graphene was grown on a copper foil (OAK-MITSUI, 99.4%) using APCVD at 1030 °C by flowing

DOI: 10.1021/acsnano.7b02182
ACS Nano XXXX, XXX, XXX−XXX

hydrogen at 10 sccm for 15 min, followed by flowing methane at 2 sccm and argon at 300 sccm for 10 min.

To transfer the graphene, sub-micrometer-thick PMMA (950 A4, MICRO-CHEM) was spin-coated on the graphene at 3000 rpm, followed by etching the copper using copper etchant and rinsing with DI water. The graphene/PMMA bilayer was then transferred onto a piece of tattoo paper (Silhouette) with graphene facing up and PMMA in contact with the paper. The Gr/PMMA bilayer was cut into serpentine ribbons using a programmable mechanical cutter plotter (Silhouette Cameo). The extraneous areas of the Gr/PMMA were manually peeled off, leaving a complete GET sensor on the tattoo paper.

Fabrication of Gr/PI Sensors. Graphene was grown on copper foil using the same method explained earlier. Next, the PI precursor (PI 2574, HD MicroSystems) was spin-coated onto the Gr/copper at a speed of 3000 rpm and cured in a vacuum oven. Then copper was etched away and the Gr/PI was transferred onto thermal release tape (TRT). The Gr/PI on TRT was cut into serpentine ribbons using a programmable mechanical cutter plotter. The Gr/PI/TRT layers were heated on a hot plate at 80 °C to decrease the adhesion strength of the TRT and allow the extraneous area to be peeled off. Finally, Gr/PI sensors were transferred to the skin with the help of medical adhesive film, Tegaderm (3M).

Experiments on Human Subjects. All experiments were conducted under approval from the Institutional Review Board at the University of Texas at Austin (protocol number: 2015-03-0082).

ASSOCIATED CONTENT

Supporting Information

The Supporting Information is available free of charge on the ACS Publications website at DOI: 10.1021/acsnano.7b02182.

Process of laminating a GET on the skin (AVI)
Performance of the GET under a cyclic tensile strain of 15% (AVI)
Video of the GET on relaxed human skin and skin subjected to various kinds of deformations (AVI)
After use, the GET can be easily peeled off from the skin by a piece of adhesive tape (AVI)
Additional figures as described in the text (PDF)

AUTHOR INFORMATION

Corresponding Authors

*E-mail (D. Akinwande): deji@ece.utexas.edu. Phone: 512-471-4345.
*E-mail (N. Lu): nanshulu@utexas.edu. Phone: 512-471-4208.

ORCID

Shideh Kabiri Ameri: 0000-0001-6931-3011

Notes

The authors declare no competing financial interest.

ACKNOWLEDGMENTS

This work is supported by the U.S. National Science Foundation (NSF) under Grant No. ECCS-1541684 and the Young Investigator Program (YIP) of the Office of Naval Research (ONR) under Grant No. N00014-16-1-2044. D.A. acknowledges the support of a David & Doris Lybarger Endowed Faculty Fellowship. We also acknowledge Professor Rodney Ruoff for the APCVD growth system.

REFERENCES

(1) Steinhubl, S. R.; Muse, E. D.; Topol, E. J. The Emerging Field of Mobile Health. *Sci. Transl. Med.* **2015**, *7*, 1−6.

(2) Evenson, K. R.; Goto, M. M.; Furberg, R. D. Systematic Review of the Validity and Reliability of Consumer-Wearable Activity Trackers. *Int. J. Behav. Nutr. Phys. Act.* **2015**, *12*.10.1186/s12966-015-0314-1

(3) Jeong, J. W.; Yeo, W. H.; Akhtar, A.; Norton, J. J. S.; Kwack, Y. J.; Li, S.; Jung, S. Y.; Su, Y. W.; Lee, W.; Xia, J.; et al. J. A. Materials and Optimized Designs for Human-Machine Interfaces *Via* Epidermal Electronics. *Adv. Mater.* **2013**, *25*, 6839−46.

(4) Searle, A.; Kirkup, L. A Direct Comparison of Wet, Dry and Insulating Bioelectric Recording Electrodes. *Physiol. Meas.* **2000**, *21*, 271−283.

(5) Gerdle, B.; Karlsson, S.; Day, S.; Djupsjöbacka, M. Acquisition, Processing and Analysis of the Surface Electromyogram. In *Modern Techniques in Neuroscience Research*; Windhorst, U., Johansson, H., Eds.; Springer: Berlin, Heidelberg, 1999; pp 705−755.

(6) Kim, D. H.; Lu, N. S.; Ma, R.; Kim, Y. S.; Kim, R. H.; Wang, S. D.; Wu, J.; Won, S. M.; Tao, H.; Islam, A.; Yu, K. J.; Kim, T. I.; Chowdhury, R.; Ying, M.; Xu, L. Z.; Li, M.; Chung, H. J.; Keum, H.; McCormick, M.; Liu, P.; et al. Epidermal Electronics. *Science* **2011**, *333*, 838−843.

(7) Jeong, J. W.; Kim, M. K.; Cheng, H. Y.; Yeo, W. H.; Huang, X.; Liu, Y. H.; Zhang, Y. H.; Huang, Y. G.; Rogers, J. A. Capacitive Epidermal Electronics for Electrically Safe, Long-Term Electrophysiological Measurements. *Adv. Healthcare Mater.* **2014**, *3*, 642−648.

(8) Webb, R. C.; Bonifas, A. P.; Behnaz, A.; Zhang, Y. H.; Yu, K. J.; Cheng, H. Y.; Shi, M. X.; Bian, Z. G.; Liu, Z. J.; Kim, Y. S.; Yeo, W. H.; Park, J. S.; Song, J. Z.; Li, Y. H.; Huang, Y. G.; Gorbach, A. M.; Rogers, J. A. Ultrathin Conformal Devices for Precise and Continuous Thermal Characterization of Human Skin. *Nat. Mater.* **2013**, *12*, 938−944.

(9) Huang, X.; Yeo, W. H.; Liu, Y.; Rogers, J. A. Epidermal Differential Impedance Sensor for Conformal Skin Hydration Monitoring. *Biointerphases* **2012**, *7*, 52.

(10) Kim, J.; Salvatore, G. A.; Araki, H.; Chiarelli, A. M.; Xie, Z. Q.; Banks, A.; Sheng, X.; Liu, Y. H.; Lee, J. W.; Jang, K. I.; Heo, S. Y.; Cho, K.; Luo, H. Y.; Zimmerman, B.; Kim, J.; Yan, L. Q.; Feng, X.; Xu, S.; Fabiani, M.; Gratton, G.; et al. Battery-Free, Stretchable Optoelectronic Systems for Wireless Optical Characterization of the Skin. *Sci. Adv.* **2016**, *2*.e160041810.1126/sciadv.1600418

(11) Bandodkar, A. J.; Jia, W. Z.; Wang, J. Tattoo-Based Wearable Electrochemical Devices: A Review. *Electroanalysis* **2015**, *27*, 562−572.

(12) Lee, H.; Choi, T. K.; Lee, Y. B.; Cho, H. R.; Ghaffari, R.; Wang, L.; Choi, H. J.; Chung, T. D.; Lu, N.; Hyeon, T.; Choi, S. H.; Kim, D. H. A Graphene-Based Electrochemical Device With Thermoresponsive Microneedles for Diabetes Monitoring and Therapy. *Nat. Nanotechnol.* **2016**, *11*, 566−572.

(13) Lu, N. S.; Yang, S. X. Mechanics for Stretchable Sensors. *Curr. Opin. Solid State Mater. Sci.* **2015**, *19*, 149−159.

(14) Wang, L.; Lu, N. Conformability of a Thin Elastic Membrane Laminated on a Soft SubstrateWith Slightly Wavy Surface. *J. Appl. Mech.* **2016**, *83*, 041007.

(15) Yeo, W.-H.; Kim, Y.-S.; Lee, J.; Ameen, A.; Shi, L.; Li, M.; Wang, S.; Ma, R.; Jin, S. H.; Kang, Z.; Huang, Y.; Rogers, J. A. Multifunctional Electronics: Multifunctional Epidermal Electronics Printed Directly Onto the Skin. *Adv. Mater.* **2013**, *25*, 2772.

(16) Geim, A. K. Graphene: Status and Prospects. *Science* **2009**, *324*, 1530−1534.

(17) Nair, R. R.; Blake, P.; Grigorenko, A. N.; Novoselov, K. S.; Booth, T. J.; Stauber, T.; Peres, N. M. R.; Geim, A. K. Fine Structure Constant Defines Visual Transparency of Graphene. *Science* **2008**, *320*, 1308−1308.

(18) Lee, C.; Wei, X. D.; Kysar, J. W.; Hone, J. Measurement of the Elastic Properties and Intrinsic Strength of Monolayer Graphene. *Science* **2008**, *321*, 385−388.

(19) Jang, H.; Park, Y. J.; Chen, X.; Das, T.; Kim, M. S.; Ahn, J. H. Graphene-Based Flexible and Stretchable Electronics. *Adv. Mater.* **2016**, *28*, 4184−4202.

(20) Ameri, S. K.; Singh, P. K.; Sonkusale, S. Utilization of Graphene Electrode in Transparent Microwell Arrays for High Throughput Cell Trapping and Lysis. *Biosens. Bioelectron.* **2014**, *61*, 625−630.

DOI: 10.1021/acsnano.7b02182
ACS Nano XXXX, XXX, XXX−XXX

(21) Ameri, S. K.; Sing, P. K.; Angelo, R. D.; Stoppel, W.; Black, L. D.; Sonkusale, S. Three Dimensional Graphene Scaffold for Cardiac Tissue Engineering and In-Situ Electrical Recording. *IEEE EMBC* **2016**, 3.420110.1109/EMBC.2016.7591653
(22) Pinto, A. M.; Goncalves, I. C.; Magalhaes, F. D. Graphene-Based Materials Biocompatibility: A review. *Colloids Surf., B* **2013**, *111*, 188−202.
(23) Mannoor, M. S.; Tao, H.; Clayton, J. D.; Sengupta, A.; Kaplan, D. L.; Naik, R. R.; Verma, N.; Omenetto, F. G.; McAlpine, M. C. Graphene-Based Wireless Bacteria Detection on Tooth Enamel. *Nat. Commun.* **2012**, 3.76310.1038/ncomms1767
(24) Kuzum, D.; Takano, H.; Shim, E.; Reed, J. C.; Juul, H.; Richardson, A. G.; de Vries, J.; Bink, H.; Dichter, M. A.; Lucas, T. H. Transparent and Flexible Low Noise Graphene Electrodes for Simultaneous Electrophysiology and Neuroimaging. *Nat. Commun.* **2014**, 5.525910.1038/ncomms6259
(25) Park, D. W.; Schendel, A. A.; Mikael, S.; Brodnick, S. K.; Richner, T. J.; Ness, J. P.; Hayat, M. R.; Atry, F.; Frye, S. T.; Pashaie, R.; Thongpang, S.; Ma, Z.; Williams, J. C. Graphene-Based Carbon-Layered Electrode Array Technology for Neural Imaging and Optogenetic Applications. *Nat. Commun.* **2014**, *5*, 5258.
(26) Lee, H.; Choi, T. K.; Lee, Y. B.; Cho, H. R.; Ghaffari, R.; Wang, L.; Choi, H. J.; Chung, T. D.; Lu, N.; Hyeon, T.; Choi, S. H.; Kim, D. H. A Graphene-Based Electrochemical Device With Thermoresponsive Microneedles for Diabetes Monitoring and Therapy. *Nat. Nanotechnol.* **2016**, *11*, 566−572.
(27) Choi, M. K.; Park, I.; Kim, D. C.; Joh, E.; Park, O. K.; Kim, J.; Kim, M.; Choi, C.; Yang, J.; Cho, K. W.; Hwang, J. H.; Nam, J. M.; Hyeon, T.; Kim, J. H.; Kim, D. H. Thermally Controlled, Patterned Graphene Transfer Printing for Transparent and Wearable Electronic/Optoelectronic System. *Adv. Funct. Mater.* **2015**, *25*, 7109−7118.
(28) Yang, S.; Chen, Y. C.; Nicolini, L.; Pasupathy, P.; Sacks, J.; Becky, S.; Yang, R.; Daniel, S.; Chang, Y. F.; Wang, P.; Schnyer, D.; Neikirk, D.; Lu, N. "Cut-and-Paste" Manufacture of Multiparametric Epidermal Sensor Systems. *Adv. Mater.* **2015**, *27*, 6423−6430.
(29) Li, X.; Cai, W.; An, J.; Kim, S.; Nah, J.; Yang, D.; Piner, R.; Velamakanni, A.; Jung, I.; Tutuc, E.; Banerjee, S. K.; Colombo, L.; Ruoff, R. S. Large-Area Synthesis of High-Quality and Uniform Graphene Films on Copper Foils. *Science* **2009**, *324*, 1312−1314.
(30) Widlund, T.; Yang, S. X.; Hsu, Y. Y.; Lu, N. S. Stretchability and Compliance of Freestanding Serpentine-Shaped Ribbons. *Int. J. Solids Struct.* **2014**, *51*, 4026−4037.
(31) Yang, S.; Qiao, S.; Lu, N. Elasticity Solutions to Nonbuckling Serpentine Ribbons. *J. Appl. Mech.* **2017**, *84*, 021004.
(32) Wang, S.; M, L., Wu, J.; Kim, D. H.; Lu, N.; Su, Y.; Kang, Z.; Huang, Y.; Rogers, J. A. Mechanics of Epidermal Electronics. *J. Appl. Mech.* **2012**, 79.03102210.1115/1.4005963
(33) Akinwande, D.; Petrone, N.; Hone, J. Two-Dimensional Flexible Nanoelectronics. *Nat. Commun.* **2014**, *5*, 5678.
(34) Arumugam, V.; Sanjeevi, R.; Naresh, M. D. Effect of Strain Rate on the Fracture Behaviour of Skin. *J. Biosci.* **1994**, *19*, 7.
(35) Liang, X.; Boppart, S. A. Biomechanical Properties of *In Vivo* Human Skin From Dynamic Optical Coherence Elastography. *IEEE Trans. Biomed. Eng.* **2010**, *57*, 953−959.
(36) Wang, L.; Lu, N. Conformability of a Thin Elastic Membrane Laminated on a Soft Substrate With Slightly Wavy Surface. *J. Appl. Mech.* **2016**, 83.04100710.1115/1.4032466
(37) Jeong, J. W.; Yeo, W. H.; Akhtar, A.; Norton, J. J.; Kwack, Y. J.; Li, S.; Jung, S. Y.; Su, Y.; Lee, W.; Xia, J.; Cheng, H.; Huang, Y.; Choi, W. S.; Bretl, T.; Rogers, J. A. Materials and Optimized Designs for Human-Machine Interfaces *Via* Epidermal Electronics. *Adv. Mater.* **2013**, *25*, 6839−6846.
(38) Chi, Y. M.; Jung, T. P.; Cauwenberghs, G. Dry-Contact and Noncontact Biopotential Electrodes: Methodological Review. *IEEE Rev. Biome. Eng.* **2010**, *3*, 106−119.
(39) Celik, N.; Manivannan, N.; Strudwick, A.; Balachandran, W. Graphene Enabled Electrodes for Electrocardiogram Monitoring. *Nanomaterials* **2016**, *6*, 156.
(40) Webster, J. G. *Medical Instrumentation Application and Design*; Wiley, 2009.
(41) Huang, X.; Cheng, H.; Chen, K.; Zhang, Y.; Zhang, Y.; Liu, Y.; Zhu, C.; Ouyang, S. C.; Kong, G. W.; Yu, C.; Huang, Y.; Rogers, J. A. Epidermal Impedance Sensing Sheets for Precision Hydration Assessment and Spatial Mapping. *IEEE Trans. Biomed. Eng.* **2013**, *60*, 2848−2857.
(42) Lee, H.; Choi, T. K.; Lee, Y. B.; Cho, H. R.; Ghaffari, R.; Wang, L.; Choi, H. J.; Chung, T. D.; Lu, N.; Hyeon, T.; Choi; Kim, D. H. A Graphene-Based Electrochemical Device With Thermoresponsive Microneedles for Diabetes Monitoring and Therapy. *Nat. Nanotechnol.* **2016**, *11*, 566−572.
(43) Yeo, W. H.; Kim, Y. S.; Lee, J.; Ameen, A.; Shi, L.; Li, M.; Wang, S.; Ma, R.; Jin, S. H.; Kang, Z.; Huang, Y.; Rogers, J. A. Multifunctional Epidermal Electronics Printed Directly Onto the Skin. *Adv. Mater.* **2013**, *25*, 2773−2778.

DOI: 10.1021/acsnano.7b02182
ACS Nano XXXX, XXX, XXX−XXX

SUPPORTING INFORMATION

Graphene Electronic Tattoo Sensors

Shideh Kabiri Ameri[1], *Rebecca Ho*[2], *Hongwoo Jang*[3], *Li Tao* [1,#], *Youhua Wang* [4], *Liu Wang* [4], *David M. Schnyer* [5], *Deji. Akinwande*[1,3]*, *Nanshu Lu*[1,2,3,4] *

[1]Deparment of Electrical and Computer Engineering, University of Texas at Austin, USA

[#]School of Materials Science and Engineering, Southeast University, Nanjing 211189, China

[2]Department of Biomedical Engineering, University of Texas at Austin, USA

[3]Texas Materials Institute, University of Texas at Austin, USA

[4]Department of Aerospace Engineering and Engineering Mechanics, University of Texas at Austin, USA

[5]Department of Psychology, University of Texas at Austin, USA

* Corresponding authors:

Deji Akinwande, deji@ece.utexas.edu, 512-471-4345, MER 1.206L, R9900, 10100 Burnet Rd. Bldg 160, Austin, TX 78758

Nanshu Lu, nanshulu@utexas.edu, 512-471-4208, 210 E. 24th St, Austin, TX 78712

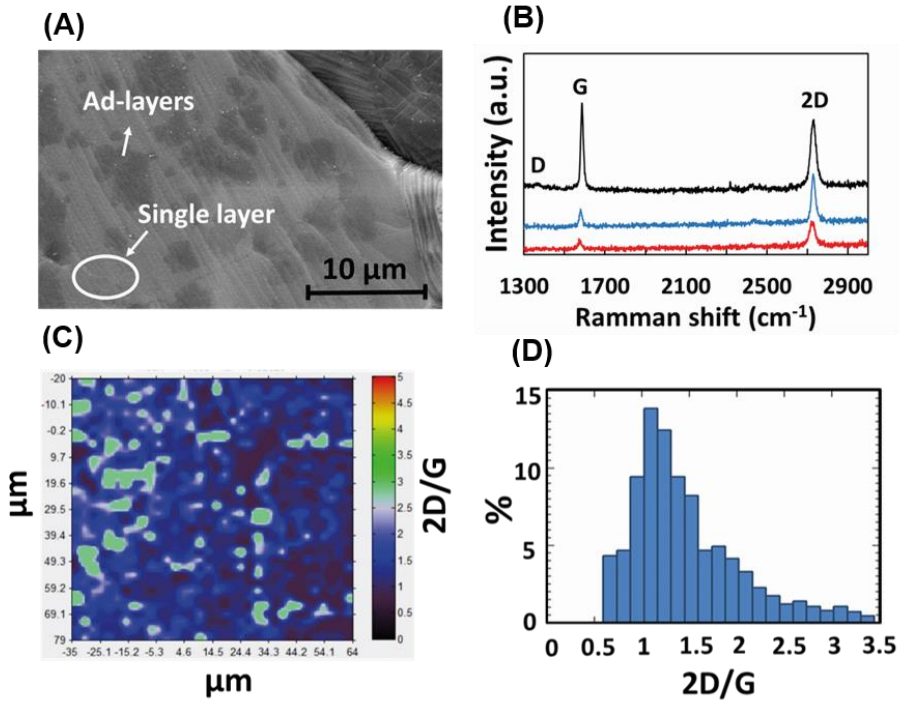

Figure S1. Scanning electron microscopy (SEM) image and Raman spectroscopy of as-grown graphene on copper. (A) SEM photo reveals the existence of ad-layers on monolayer CVD graphene. (B) Raman spectroscopy of the graphene. Blue, red and black curves were measured at different spots on the graphene. (C) Raman mapping over an area of 100 µm × 100 µm with resolution of 3 µm. The values of 2D/G ratio were denoted by different colors, which indicates the number of layers. (D) Histogram of the 2D/G ratio, suggesting that roughly 60% to 70% of the area is monolayer graphene.

Fabrication process of graphene/polyimide (Gr/PI) sensors

To study the effect of sensor thickness on its functionality, we fabricated graphene sensors using 13-µm-thick polyimide (PI) support instead of 500-nm-thick PMMA. The fabrication process of graphene/polyimide (Gr/PI) sensors is illustrated in Fig. S2. First, graphene was grown on copper foil using APCVD. Then liquid polyimide (PI 2574, HD Microsystems) was spin-coated on graphene and cured in vacuum oven. In the next step, copper was etched away and Gr/PI bilayer was transferred to a thermal release tape (TRT) while graphene was faced up. Thereafter, Gr/PI bilayer was cut to the same patterns as Gr/PMMA (GET) using the Silhouette Cameo mechanical cutter plotter. Gr/PI/TRT was heated at100 ℃ for about 3 minutes followed by peeling the extraneous areas. Finally, the Gr/PI sensors were transferred on a Tegaderm tape to for lamination on skin.

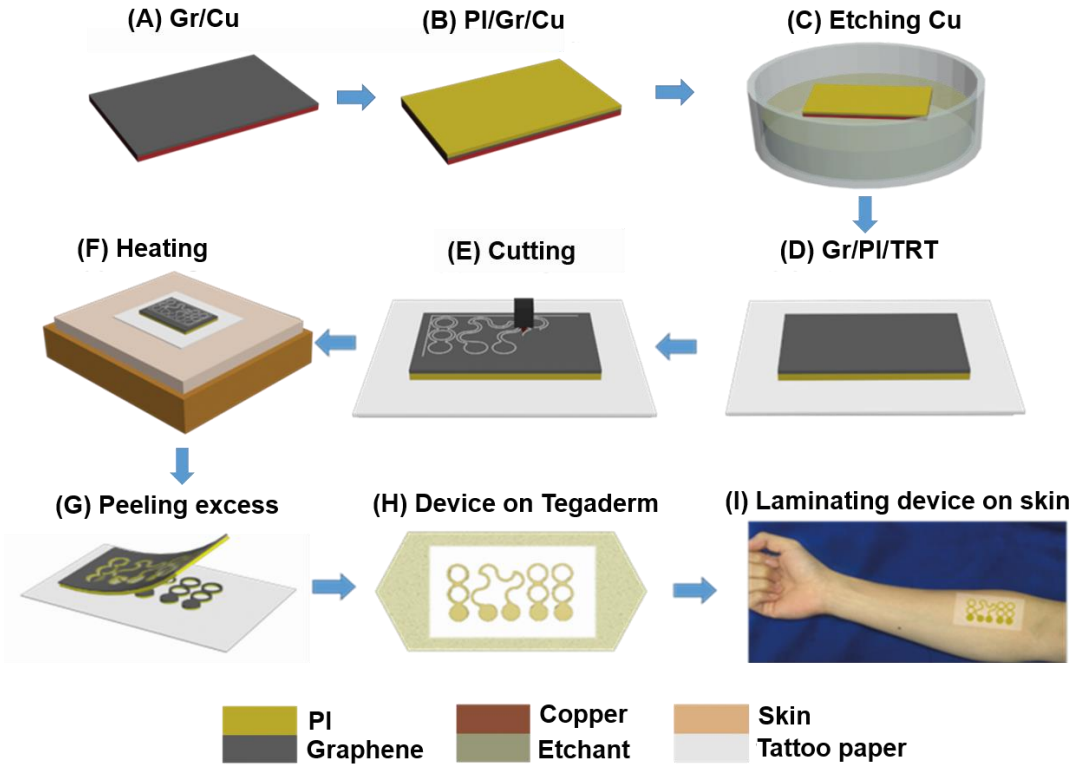

Figure S2. Fabrication process of Gr/PI sensors. (A) Graphene was grown by atmospheric pressure chemical vapor deposition system (APCVD) on a copper foil. (B) Polyamide precursor was spin-coated on graphene and cured in vacuumed oven. (C) The copper foil was etched away. (D) Gr/PI bilayer was transferred on a thermal releasing tape (TRT) with graphene facing up. (E) The bilayer was patterned using cutting machine. (F) The Gr/PI/TRT was heated at 100°C on a hot plate. (G) The excess was peeled off. (H) The device was transferred on Tegaderm. (I) The Gr/PI was mounted on human skin.

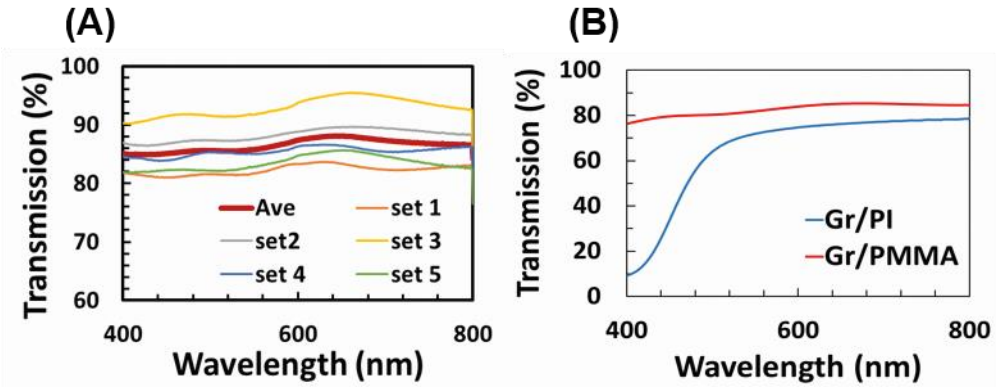

Figure S3. Optical transmission of Gr/PMMA and Gr/PI measured by Varian Cary 5G UV-VIS-NIR spectrophotometer. (A) Optical transmission of Gr/PMMA measured at 5 random spots. The averaged transmission spectra has been plotted as well. (B) Optical transmission of the Gr/PMMA and Gr/PI was compared over the wavelength from 400nm to 800nm.

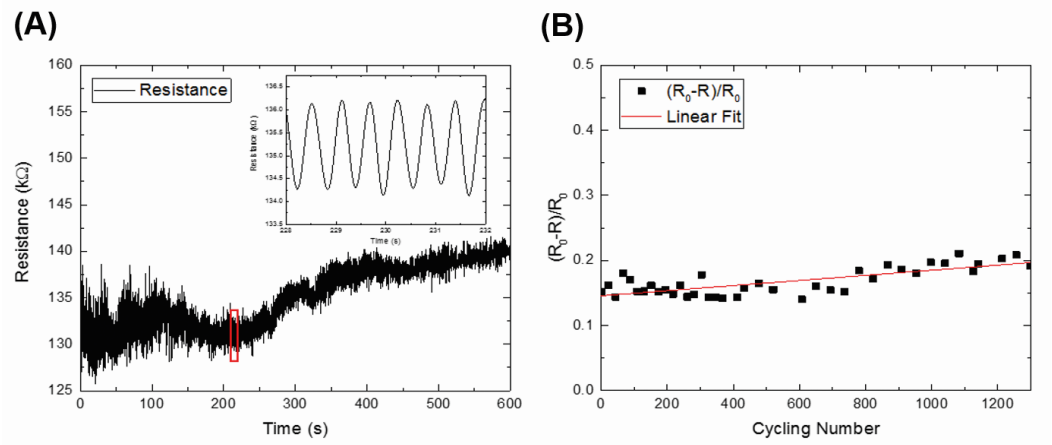

Figure S4. Cyclic test of GET on a skin replica under 15% applied strain. (A) Resistance change of GRTD up to 1300 cycles. (B) The zoomed-in resistance of the red box in Fig. S4A.

Analytical model of GET conformability on skin:

The conformability of GET on human skin can be predicted by the energy minimization method proposed by Liu *et al.*[1] The total energy of GET-skin system can be expressed as

$$U_{total} = U_{bending} + U_{adhesion} + U_{skin}$$

where $U_{bending}$ is the bending energy of the GET, $U_{adhesion}$ is the interface adhesion energy between GET and the human skin, and U_{skin} is the elastic energy stored in the deformed skin. Reasonable parameters to be used in this model are listed in Table S1.

Table S1. Detailed mechanical parameters used in energy minimization method.

Model parameter	**Value**
Graphene-skin work of adhesion (γ)	18 mJ·m^{-2} [2]
Plane strain modulus of human skin ($\bar{E}_s$)	130 kPa [3]
Human skin roughness wavelength (λ)	250 μm [4]
Human skin roughness amplitude (h)	50 μm [5]
Plane strain modulus of PMMA ($\bar{E}_m$)	3.3 GPa

Our model predicts that GET has to be thinner than 510 nm to achieve full conformability, as shown in Fig. S5. Since GET thickness was measured to be 463 ± 30 nm, it is predicted to fully conform to skin morphology, which is validated by experimental micrographs in Figs. 2j-2l. Gr/PI, however, is 13-μm-thick and thus far from being able to conform. Therefore Gr/PI requires Tegaderm tape to hold it on skin.

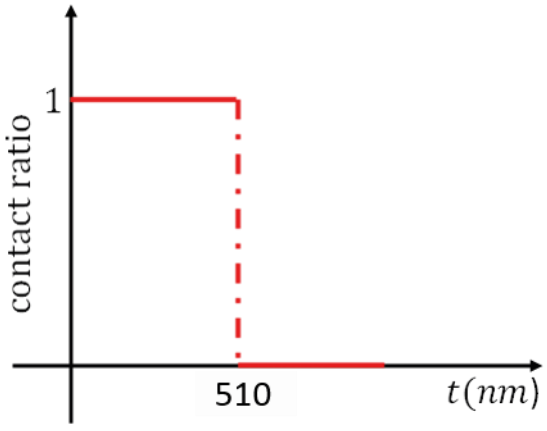

Figure S5. The plot of conformability versus the thickness of graphene sensors. Our model suggests that full conformability can only be achieved by sensors thinner than 510 nm.

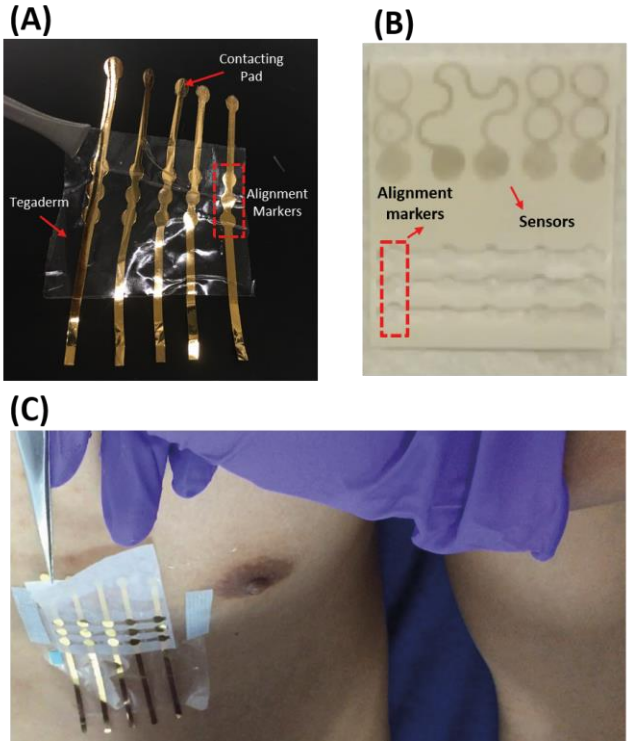

Figure S6. Customized flexible connector. (A) A five channel flexible connector made by cutting 100-nm-thick gold on 13-µm-thick PET. The boxed feature in every ribbon was used as alignment markers used to align it with GET on skin. (B) GET on tattoo paper. Alignment markers are cut open. (C) Flexible connectors were first fixed on skin, followed by placing GET on skin and aligning it with the connecters.

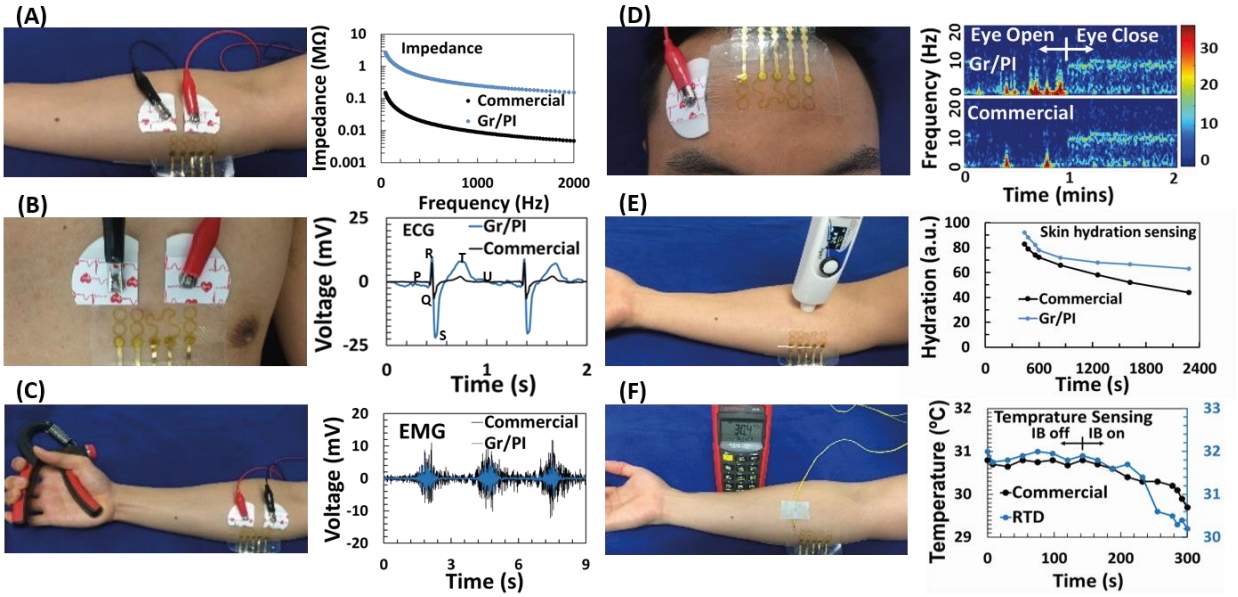

Figure S7. Functionalities of Gr/PI sensors. (A) Gr/PI-skin contact impedance compared with commercial-gel-skin impedance, which indicates non-conformal contact with skin. (B) EEG measurement using Gr/PI sensor and commercial electrodes. Gr/PI spectrogram is noisier than gel electrodes. (C) ECG recorded using Gr/PI and gel electrodes. (D) EMG captured by Gr/PI and gel electrodes. (E) Skin hydration sensing after applying body lotion on skin. The slower decay measured by Gr/PI may be attributed to the coverage of Tegaderm, which limits the breathability of skin covered by the sensor. (F) Skin temperature sensing. IB stands for ice bag which was placed in vicinity of Gr/PI to regulate skin temperature.

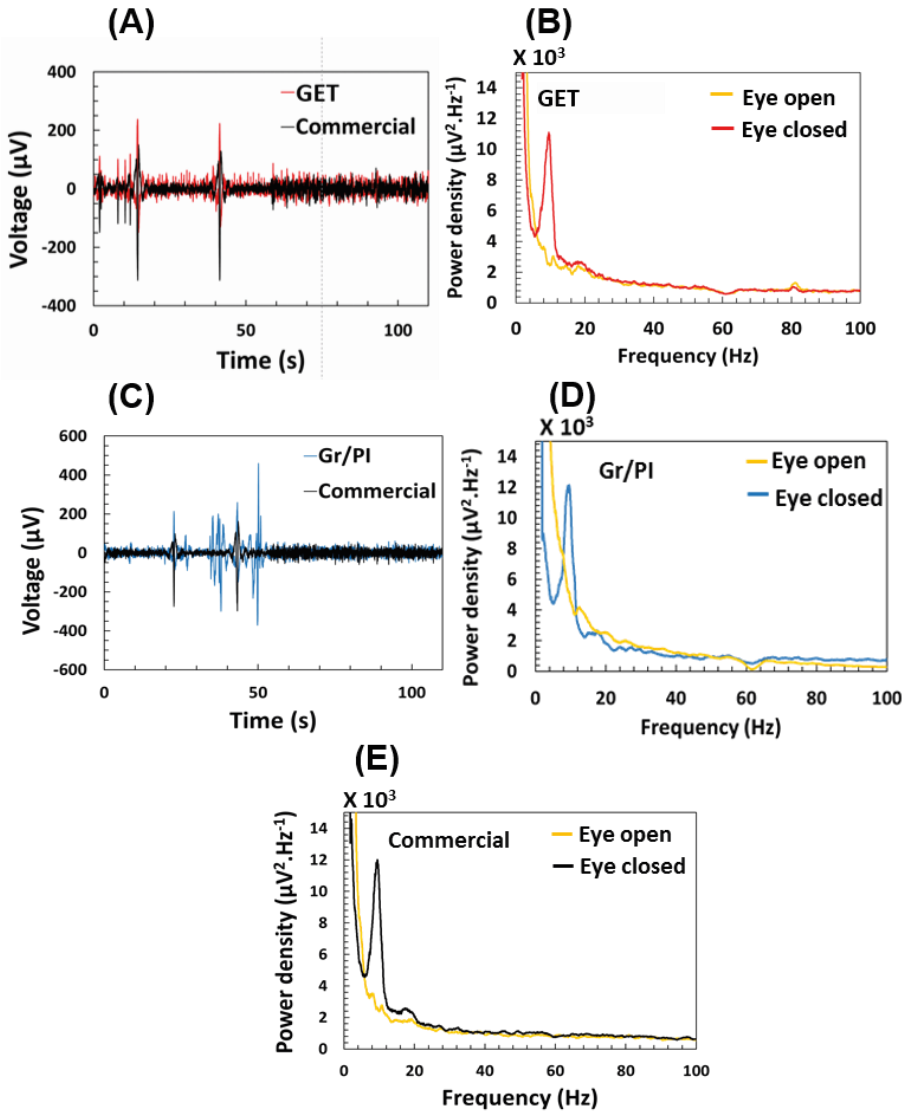

Figure S8. EEG signals in time and frequency domains. Raw EEG data and the corresponding fast Fourier transform (FFT) recorded using GET and Gr/PI and the commercial electrode. (A) The raw EEG signals from the GET closely matches that from commercial gel electrodes. (B) The FFT of EEG signals recorded using GET. (C) The raw EEG signals recorded using Gr/PI show more motion artifacts than that from the gel electrodes. (D&E) The FFT of EEG signals recorded using Gr/PI and commercial gel electrodes. Although *α* rhythm is visible in all three spectra, the GET spectrum is more similar to that of the gel electrode.

Circuit model for electrode-skin interface

The conformability ratio has been defined as the ratio of electrode come in direct contact with skin over total electrode area, in this model. Skin electrical parameters such as resistance and capacitance at electrode-skin interface are obtained from literatures as listed in Table S2. Figure S9A-D illustrate the schematic and circuit model for conformal and non-conformal electrode-skin contact. The air gaps which usually form between non-conformal electrode and skin have been shown and modeled in Fig. S9B&D. Microwave Office was used to simulate the variation of output signal strength as a result of enhancement of conformability. Simulation results in Fig. S9E clearly show that the signal loss decreases as conformability improves. Therefore, high conformability results in high signal-to-noise ratio (SNR). The result of our modeling is consistent with our experimental findings which indicate the GET-skin impedance is closely comparable with that of gel-skin impedance (Fig. 3A) whereas the Gr/PI-skin impedance is more than one order higher (Fig. S7A). Our experiments also yield higher SNR of ECG signal measured by GET (15.22 dB) than that measured by Gr/PI electrodes (7.2 dB).

Table S2. The skin model parameters and values used in simulation.

Model parameters	**Values**
Skin epidermis resistance (R_{se})	100 KΩ [6]
Skin epidermis capacitance (C_{se})	4 nF [6]
Skin dermis and subcutaneous resistance (R_{sd})	326 Ω [6]
Gap resistance (R_g)	2.9 TΩ [7]
Gap capacitance (C_g)	0.43 nF
Electrode area	0.245 cm^2

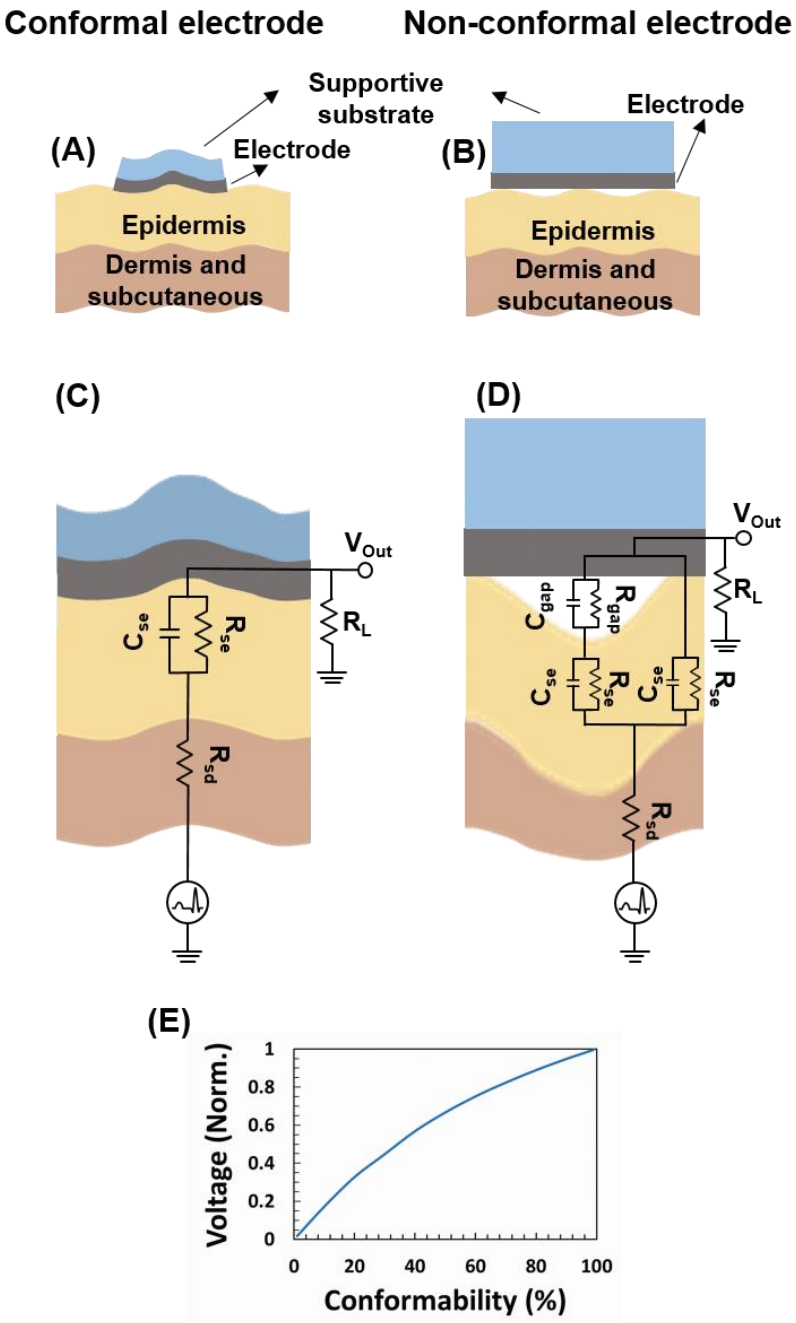

Figure S9. Electrical circuit models and simulation results of conformed and non-conformed dry electrodes to skin. Schematics showing (A) fully conformed and (B) non-conformed dry electrodes on skin. (C) Circuit model of fully conformed dry electrode where only dermis resistance (R_{sd}), epidermis resistance (R_{se}) and capacitance (C_{se}) need to be considered. (D) Circuit model of non-conformed dry electrode where the air gap contributes to extra C_{gap} and R_{gap} and hence higher interface impedance. (E) Simulation result from Microwave Office shows that the strength of the electrical signal increases as electrode-skin conformability increases. The height of the gap is assumed to be 50 μm in the simulation[5].

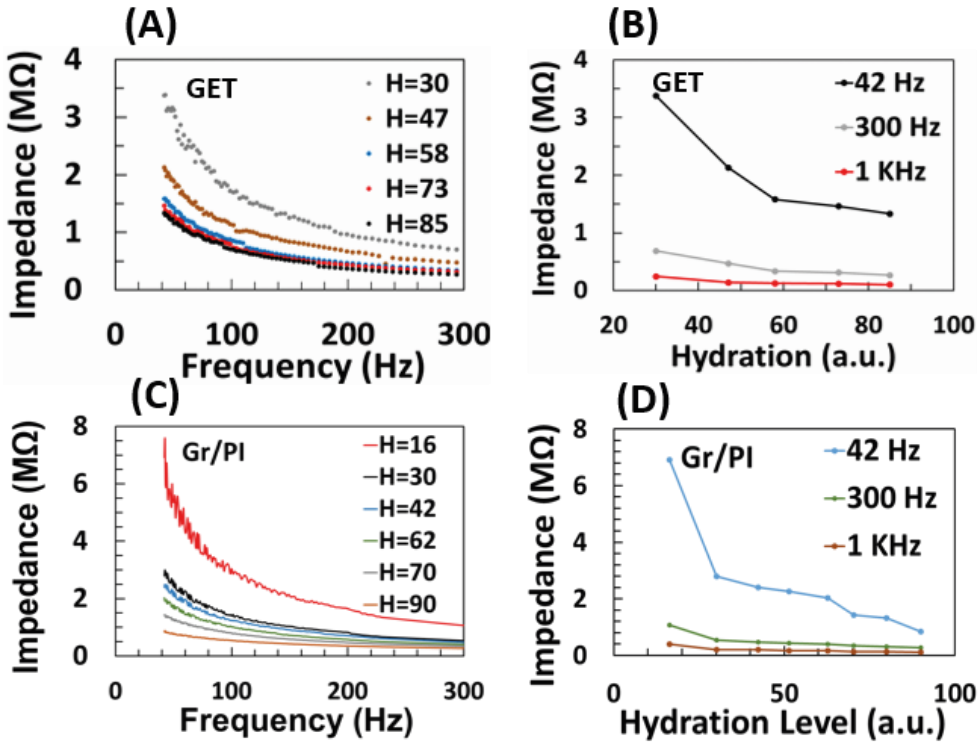

Figure S10. Calibration of skin hydration sensors of GET and Gr/PI sensor systems. Actual skin hydration was measured by commercial corneometer. Body lotion was applied to tune skin hydration. (A&B) Skin impedance measured by GET at different hydration levels and frequencies. (C&D) Skin impedance measured by Gr/PI electrodes at different hydration levels and frequencies.

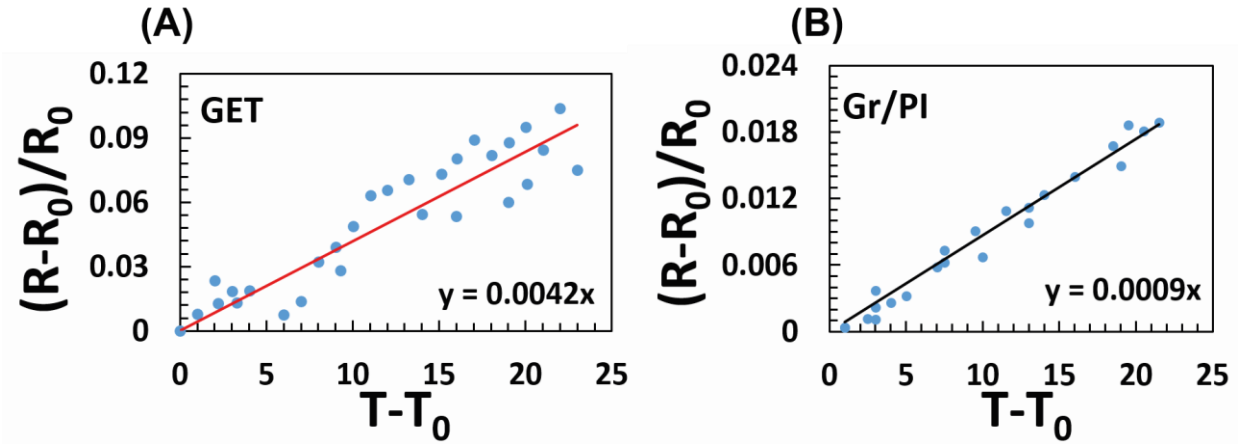

Figure S11. Calibration of RTDs of GET and Gr/PI sensor systems on hotplate. Actual temperature was measured by commercial thermocouples. Normalized resistance change as a function of temperature change plotted for (A) GRTD and (B) Gr/PI based RTD. The resistance of both RTDs increases with increasing temperature. The temperature coefficient of resistance of GET and Gr/PI were found to be 0.0042 and 0.0009, respectively. The discrepancy indicates that the behavior of graphene-based RTD is significantly affected by its supporting substrate.

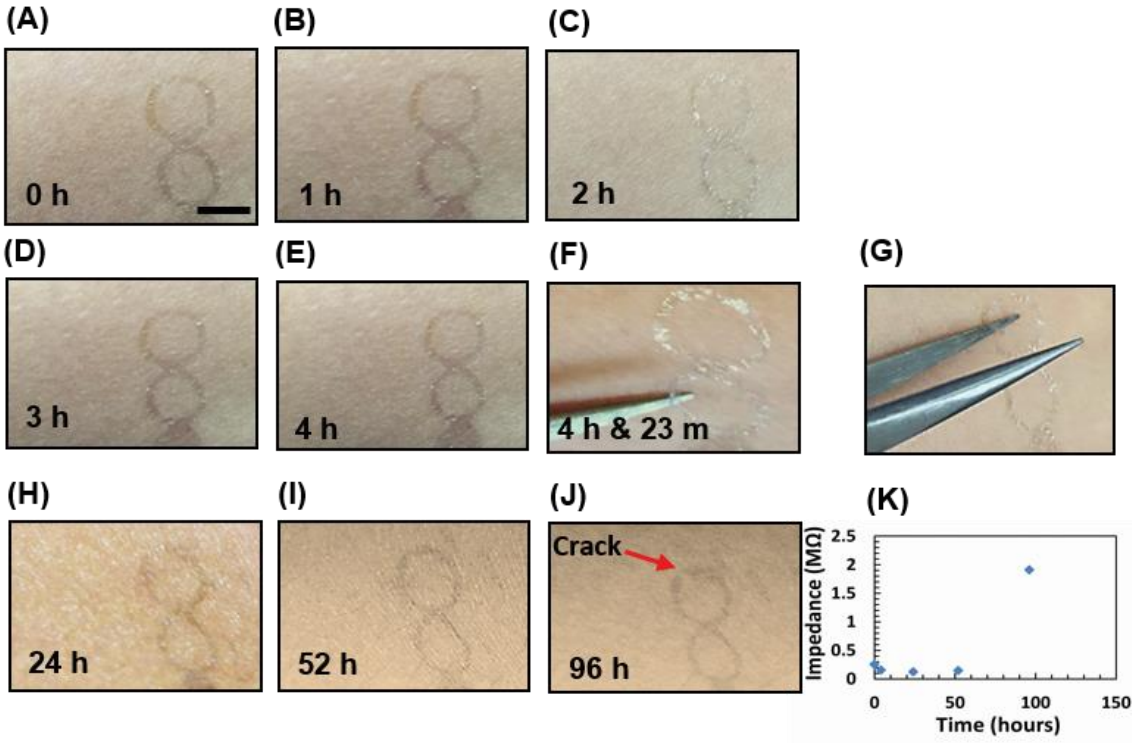

Figure S12. Wearability and durability of GET. (A to E) Photographs of GET on skin without application of any adhesive. The scale bar represents 5 mm. (F) First delamination was observed at 4 hours and 23 minutes after GET was transferred on skin. (G) First rupture was observed 5 hours after the transfer. (H to J) Liquid bandage was used to cover GET, cracks were observed 96 hours after transfer. (K) GET-skin contact impedance escalated when GET ruptured.

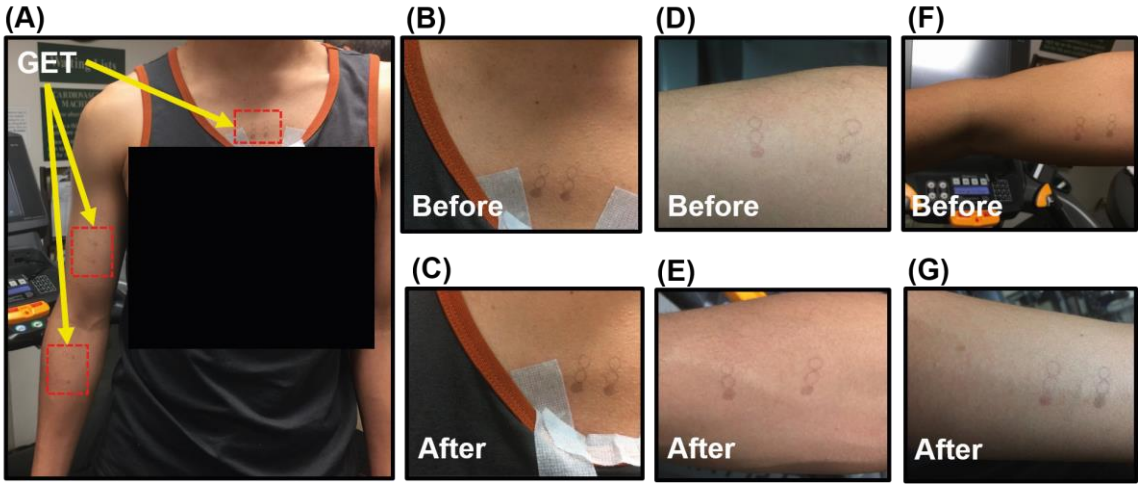

Figure S13. The effect of exercise and sweat on GET durability. (A) Three GEPSs were applied at three different locations of the subject's skin. The subject then ran on treadmill for 25 minutes at 6.5 mph. Photographs of the three GEPSs before and after the exercise. GEPSs on chest (B&C), forearm (D&E) and bicep (F&G) were not affected by the exercise or sweat.

REFERENCES

(1) Wang, L.; Lu, N. Conformability of a Thin Elastic Membrane Laminated on a Soft Substrate with Slightly Wavy Surface. *J. Appl. Mech.* **2016**, 83, 041007.

(2) Shih, C. J.; Strano, M. S.; Blankschtein, D. Wetting Translucency of Graphene. *Nat. Mater.* **2013**, 12, 866-869.

(3) Pailler-Mattei, C.; Bec, S.; Zahouani, H. *In vivo* Measurements of the Elastic Mechanical Properties of Human Skin by Indentation Tests. *Med. Eng. Phys.* **2008**, 30, 599-606.

(4) Jeong, J.-W.; Yeo, W.-H.; Akhtar, A.; Norton, J. J. S.; Kwack, Y.-J.; Li, S.; Jung, S.-Y.; Su, Y.; Lee, W.; Xia, J.; at al. Materials and Optimized Designs for Human-Machine Interfaces *Via* Epidermal Electronics. *Adv. Mate.r* **2013**, 25, 6839-6846.

(5) Tchvialevaa, L.; Zenga, H.; Markhvidaa, I.; McLeana, D. I.; Luia, H.; Leea, T. K. Skin Roughness Assessment, New Developments in Biomedical Engineering. *Domenico Campolo (Ed.), InTech* DOI: 10.5772/7611.

(6) Dorgan, S. J.; Reilly, R. B. A Model for Human Skin Impedance During Surface Functional Neuromuscular Stimulation. *Conf. Proc. IEEE Eng. Med. Bio.l Soc.* **1999**, 7, 341-348.

(7) Kamra, A. K.; Deshpande, C. G.; Gopalakrishnan, V. Effect of Relative Humidity on the Electrical Conductivity of Marine Air. *Q. J. R. Meteorol. Soc.* **1997**, 123, 16.